A simple unsymmetric 4-node 12-DOF membrane element for the modified couple stress theory

Yan Shang[1], Zheng-Hua Qian[1], Song Cen[2], Chen-Feng Li[3]

[1]*State Key Laboratory of Mechanics and Control of Mechanical Structures, College of Aerospace Engineering, Nanjing University of Aeronautics and Astronautics, Nanjing 210016, China*

[2]*Department of Engineering Mechanics, School of Aerospace Engineering, Tsinghua University, Beijing 100084, China*

[3]*Zienkiewicz Centre for Computational Engineering and Energy Safety Research Institute, College of Engineering, Swansea University, Swansea SA2 8PP, UK*

SUMMARY

In this work, the recently proposed unsymmetric 4-node 12-DOF (degree of freedom) membrane element [1], which has demonstrated excellent performance for the classical elastic problems, is further extended for the modified couple stress theory, to account for the size-effect of materials. This is achieved via two formulation developments. First, by using the penalty function method, the kinematic relations between the element's nodal drilling DOFs and the true physical rotations are enforced. Consequently, the continuity requirement from the modified couple stress theory is satisfied in weak sense, and the symmetric curvature test function can be derived from the gradients of the drilling DOFs. Secondly, the couple stress field that satisfies *a priori* the related equilibrium equations is adopted as the energy conjugate trial function to formulate the element for the modified couple stress theory. As demonstrated by a series of benchmark tests, the new element can efficiently capture the size-dependent responses of materials and is robust to mesh-distortion. Moreover, as the new element uses only three conventional DOFs per node, it can be readily incorporated into the standard finite element framework and commonly available finite element programs.

KEY WORDS: finite element method; unsymmetric; size effect; modified couple stress theory; penalty function

1. Introduction

There is mounting evidence for strong size effects of materials, especially when the deformation takes place at the microscale or below. For instance, Fleck et al. [2] conducted a torsion test on copper wires and discovered the shear strength increases as the wire diameter decreases; Lam et al.

[3] reported the flexural rigidity of a micro epoxy beam varies with respected to the structure size. Similar phenomena have also been observed in other experiments [4-8]. The classical continuum theory cannot capture such size effects, because it assumes the material is homogeneous and only the force can be transmitted to infinitesimal surfaces, which may no longer be valid at small length scales. New continuum theories are needed to describe these size-dependent deformation behaviors.

Since the pioneering work of Cosserat brothers [9], substantial efforts have been made to investigate the size effects related to material deformation, resulting in a diverse range of continuum theories. Mindlin [10] developed a microstructure theory that contains eighteen material constants for an isotropic material, and it was later simplified into the strain gradient theory [11] that contains two Lamé coefficients and five additional material constants. Fleck and Hutchinson [12] extended this theory into the plastic strain gradient theory. Aifantis [13] also developed a non-local theory for plastic materials. Lam et al. [3] modified the strain gradient theory so that it only requires three additional material constants. Also, by eliminating the difference between micro-rotation and macro-rotation in the Cosserat theory [9], Koiter [14], Mindlin and Tiersten [15] and Toupin [16] proposed the couple stress theory that contains only two additional constants, which has been proved to be a special case of the strain gradient theory [11].

To support practical use in engineering applications, many attempts [17-21] have been made to further reduce the number of additional material constants required to describe the size-dependent behavior. Among them, Yang et al. [21] proposed the modified couple stress theory, in which only the symmetric terms of curvatures are considered for contribution to the deformation energy. The modified couple stress theory requires just one additional material parameter to describe the size-dependent deformation, and has become increasingly popular in recent years due to its simplicity and verifiability.

It is hard to solve analytically the size-effect related problems, because the size-dependent continuum theories are much more complicated than the classical elasticity theory. The finite element method (FEM), which is generally regarded as the most efficient and popular numerical tool for modelling solids [22], provides a promising solution [23-27]. However, due to the presence of the second-order derivatives of displacements in these size-dependent continuum theories, the displacement-based FEM simulation requires C^1 continuity for the displacement interpolation. This brings a significant challenge to the element construction and complicates the element formulation.

For instance, Zervos et al. [28] and Papanicolopulos et al. [29] developed strict C^1 elements for the strain gradient theory but due to some inherent drawbacks [30], these complex C^1 elements can only be used in certain restricted cases.

Alternatively, Ma and Chen [31, 32] developed 3-node triangular and 4-node quadrilateral hybrid stress element models which have six DOFs (degrees of freedom) per node, including two displacements and four displacement derivatives. In these hybrid elements, the C^1 continuity requirement is satisfied in weak sense. Zhao et al. [33, 34] and Wang et al. [35, 36] also proposed similar elements based on the refined nonconforming element method and the quasi-conforming element method, respectively. However, such treatments with both displacements and their gradients taken as nodal DOFs may significantly increase the computational cost at the element level. Moreover, it is inconvenient to incorporate such elements into the standard FEM framework or commercial FEM software. An effective approach to simplify the element formulation is to introduce the independent rotation or drilling DOFs [37, 38]. In this approach, the penalty function method [39, 40] or the Lagrangian multiplier method [30, 41] is usually employed to constrain the kinematic relations between the independent rotation DOFs and the physical rotations derived from displacements, so that the C^1 continuity requirement is met in weak sense.

Recently, Shang and Ouyang [1] proposed a simple and robust 4-node 12-DOF quadrilateral membrane element US-Q4θ for the classical elastic problems based on the unsymmetric finite element method [42-44]. The unsymmetric FEM, which has been successfully applied to various applications in past years [45-49], employs different interpolations for the test and trial functions in the element formulation. Demonstrated by numerical tests [1], the element US-Q4θ exhibits good numerical accuracy and resistance to mesh distortions, even when the element shape is severely distorted into concave quadrilateral or triangle. In this work, the unsymmetric US-Q4θ element, originally designed for classical elastic problems, is further developed to model size-dependent material responses based on the modified couple stress theory [21]. Since the US-Q4θ element uses the drilling DOFs, the key step here is to introduce a proper penalty function to ensure the nodal drilling DOFs effectively approximates the true physical rotations. Then, the test function for the symmetric curvature in the virtual work principle can be readily determined as the derivatives of these drilling DOFs. Meanwhile, the trial function for the couple stress, which conjugates with the curvature test function, can be directly formulated following the analytical trial function method [50]

and the quasi-conforming technique [51, 52]. Developed for the modified couple stress theory, the new element, renamed as US-Q4θ-CS, is expected to work with size-dependent problems with good numerical precision and high resistance to mesh distortion. Moreover, as the new element still has only two translational DOFs and one drilling DOF per node, it can be easily incorporated into the standard FEM framework and commercial FEM software.

The remainder of this paper is organized as follows. The modified couple stress theory proposed in [21] is briefly reviewed in Section 2. Next, the element formulation is explained in Section 3 and several numerical benchmark tests are presented in Section 4 to validate the new element's capacity. Finally, some conclusions and discussions are drawn in Section 5.

2. Overview of Modified Couple Stress Elasticity Theory

2.1. General governing equations

In the modified couple stress theory [21], the strain components ε_{ij} and the rotation components ω_i are defined as the spatial derivatives of displacement u_i:

$$\varepsilon_{ij} = \frac{u_{i,j} + u_{j,i}}{2}, \quad \omega_i = \frac{1}{2} e_{ijk} u_{k,j}, \tag{1}$$

where e_{ijk} is the Levi-Civita symbol. Different from the classical couple stress theories [14-16] in which both symmetric and anti-symmetric parts of rotation gradients contribute to the deformation energy, only the symmetric part is considered in Yang's modified couple stress theory [21]. Then, the symmetric curvature components χ_{ij} are defined as

$$\chi_{ij} = \frac{\omega_{i,j} + \omega_{j,i}}{2}. \tag{2}$$

For a linear elastic isotropic material, the stress σ_{ij} and the couple stress m_{ij}, which are work conjugates of the above strain and curvature respectively, can be obtained using the constitutive relations:

$$\sigma_{ij} = \lambda \varepsilon_{kk} \delta_{ij} + 2G\varepsilon_{ij}, \quad m_{ij} = 2Gl^2 \chi_{ij}, \tag{3}$$

in which λ and G are the two Lamé constants in Cauchy elasticity, l the additional material length scale parameter, and δ_{ij} the Kronecker delta. The higher-order equilibrium equations are expressed as

$$\sigma_{ik,i} - \frac{1}{2} e_{jlk} m_{ij,il} + f_k = 0 , \tag{4}$$

where f_k denotes the body force per unit volume. The body couple force is not included in Equation (4), because it can be decomposed into an equivalent system of body force and surface force [53].

2.2. Two-dimensional problem

As discussed in [54], the curvature terms produced by the thickness-direction displacement contribute to the deformation energy in the modified couple stress theory, therefore the plane stress state cannot be accurately simulated through a two-dimensional simplification. Thus, only the plane strain state is considered in this work.

In the following sections, *x*- and *y*- are used to represent the two in-plane directions, while *z*- refers to the thickness direction. Correspondingly, the three displacement components are denoted as *u*, *v* and *w*, respectively. Under the plain strain assumption, the nonzero strain and curvature terms can be expressed in the following vector forms:

$$\boldsymbol{\varepsilon} = \begin{Bmatrix} \varepsilon_x \\ \varepsilon_y \\ \gamma_{xy} \end{Bmatrix} = \begin{Bmatrix} \dfrac{\partial u}{\partial x} \\ \dfrac{\partial v}{\partial y} \\ \dfrac{\partial u}{\partial y} + \dfrac{\partial v}{\partial x} \end{Bmatrix}, \tag{5}$$

$$\boldsymbol{\chi} = \begin{Bmatrix} 2\chi_{xz} \\ 2\chi_{yz} \end{Bmatrix} = \begin{Bmatrix} \dfrac{\partial \omega_z}{\partial x} \\ \dfrac{\partial \omega_z}{\partial y} \end{Bmatrix}, \tag{6}$$

in which

$$\omega_z = \frac{1}{2}\left(\frac{\partial v}{\partial x} - \frac{\partial u}{\partial y} \right). \tag{7}$$

The coefficient “2” in Equation (6) is to consider the symmetry of the curvatures. The stress and couple stress can be obtained by using the constitutive equations:

$$\boldsymbol{\sigma} = \begin{Bmatrix} \sigma_x \\ \sigma_y \\ \sigma_{xy} \end{Bmatrix} = \mathbf{D}_n \boldsymbol{\varepsilon} , \tag{8}$$

$$\mathbf{m} = \begin{Bmatrix} m_{xz} \\ m_{yz} \end{Bmatrix} = \mathbf{D}_c \boldsymbol{\chi} , \tag{9}$$

with

$$\mathbf{D}_n = \frac{E}{(1+\nu)(1-2\nu)} \begin{bmatrix} 1-\nu & \nu & 0 \\ \nu & 1-\nu & 0 \\ 0 & 0 & (1-2\nu)/2 \end{bmatrix}, \tag{10}$$

$$\mathbf{D}_c = \begin{bmatrix} Gl^2 & 0 \\ 0 & Gl^2 \end{bmatrix}, \tag{11}$$

in which E denotes Young's modulus, ν Poisson's ratio and $G = E/2(1+\nu)$.

3. Finite Element Formulation

3.1. Virtual work principle for unsymmetric FEM

The unsymmetric FEM is developed following the virtual work principle and it employs different interpolations for the element test and trial functions. With respect to the proposed membrane element model for the modified couple stress theory, the virtual work principle incorporating the penalty term can be expressed as

$$\begin{aligned} \iint_\Omega \delta\bar{\boldsymbol{\varepsilon}}^{\mathrm{T}} \hat{\boldsymbol{\sigma}} t \mathrm{d}\Omega + \iint_\Omega \delta\bar{\boldsymbol{\chi}}^{\mathrm{T}} \hat{\mathbf{m}} t \mathrm{d}\Omega - \iint_\Omega \delta\bar{\mathbf{u}}^{\mathrm{T}} \mathbf{f} t \mathrm{d}\Omega - \int_\Gamma \delta\bar{\mathbf{u}}^{\mathrm{T}} \mathbf{R} t \mathrm{d}\Gamma \\ - \int_\Gamma \delta\bar{\omega}_z M_z t \mathrm{d}\Gamma + k \iint_\Omega \delta\Lambda \Lambda t \mathrm{d}\Omega = 0 \end{aligned} , \tag{12}$$

in which Ω is the domain bounded by Γ; t is thickness; $\mathbf{f}$ denotes the body force vector; $\mathbf{R}$ and M_z represent respectively the prescribed external force and couple force at the boundary; $\bar{\mathbf{u}}$ is the test function for displacement, and $\bar{\boldsymbol{\varepsilon}}$ and $\bar{\boldsymbol{\chi}}$ are the test functions for strain and symmetric curvature; $\bar{\omega}_z$ is the test function for the physical rotation, independently interpolated by the element nodal drilling DOFs; $\hat{\boldsymbol{\sigma}}$ and $\hat{\mathbf{m}}$ are the trial functions for stress and couple stress, respectively.

Moreover, the last term in Equation (12) is the penalty function term, which constrains the kinematic relations between the independently assumed rotation $\bar{\omega}_z$ and the one derived from displacement $\bar{\mathbf{u}}$. By adding the penalty function term, the rotation $\bar{\omega}_z$ can effectively reproduce the true physical rotation. This will be discussed in more details in Section 3.2.3.

3.2. The new unsymmetric element US-Q4θ-CS

As stated above, the proposed element is directly developed from the existing high-performance 4-node element US-Q4θ [1] which is proposed for classical elastic problems. As shown in Figure 1, the new element still has three DOFs per node:

$$\mathbf{q}^e = \begin{bmatrix} u_1 & v_1 & \theta_1 & u_2 & v_2 & \theta_2 & u_3 & v_3 & \theta_3 & u_4 & v_4 & \theta_4 \end{bmatrix}^{\mathrm{T}}. \tag{13}$$

3.2.1 The element's test functions

In this work, the test function for displacement is also determined by using the concise interpolations proposed in [1], which can meet the requirements of interelement compatibilities for any distorted geometry:

$$\bar{\mathbf{u}} = \begin{Bmatrix} \bar{u} \\ \bar{v} \end{Bmatrix} = \bar{\mathbf{N}}\mathbf{q}^e, \tag{14}$$

with

$$\bar{\mathbf{N}} = \begin{bmatrix} \bar{\mathbf{N}}_1 & \bar{\mathbf{N}}_2 & \bar{\mathbf{N}}_3 & \bar{\mathbf{N}}_4 \end{bmatrix}, \tag{15}$$

$$\bar{\mathbf{N}}_i = \begin{bmatrix} N_i & 0 & -\dfrac{1}{2}N_i\left(y - y_i\right) \\ 0 & N_i & \dfrac{1}{2}N_i\left(x - x_i\right) \end{bmatrix}, \quad i = 1 \sim 4, \tag{16}$$

where $\left(x_i, y_i\right)$ are the Cartesian coordinates of node *i*; N_i $\left(i = 1 \sim 4\right)$ are the shape functions of the standard 4-node isoparametric element:

$$\begin{cases} N_1 = \dfrac{1}{4}(1-\xi)(1-\eta), & N_2 = \dfrac{1}{4}(1+\xi)(1-\eta) \\ N_3 = \dfrac{1}{4}(1+\xi)(1+\eta), & N_4 = \dfrac{1}{4}(1-\xi)(1+\eta) \end{cases}, \tag{17}$$

in which $\left(\xi, \eta\right)$ are the isoparametric coordinates. Then, by substituting Equation (14) into the displacement-strain equations, the test function for strain can be obtained:

$$\bar{\boldsymbol{\varepsilon}} = \begin{Bmatrix} \bar{\varepsilon}_x \\ \bar{\varepsilon}_y \\ \bar{\gamma}_{xy} \end{Bmatrix} = \bar{\mathbf{B}}^n\mathbf{q}^e, \tag{18}$$

with

$$\bar{\mathbf{B}}^n = \left[\bar{\mathbf{B}}_1^n \quad \bar{\mathbf{B}}_2^n \quad \bar{\mathbf{B}}_3^n \quad \bar{\mathbf{B}}_4^n \right], \tag{19}$$

$$\bar{\mathbf{B}}_i^n = \begin{bmatrix} N_{i,x} & 0 & -\frac{1}{2} N_{i,x} \left(y - y_i \right) \\ 0 & N_{i,y} & \frac{1}{2} N_{i,y} \left(x - x_i \right) \\ N_{i,y} & N_{i,x} & \frac{1}{2} N_{i,x} \left(x - x_i \right) - \frac{1}{2} N_{i,y} \left(y - y_i \right) \end{bmatrix}, \quad i = 1 \sim 4 . \tag{20}$$

As previously discussed, $\bar{\omega}_z$ is independently interpolated by the element nodal drilling DOFs:

$$\bar{\omega}_z = \bar{\mathbf{N}}^{\omega} \mathbf{q}^e , \tag{21}$$

with

$$\bar{\mathbf{N}}^{\omega} = \begin{bmatrix} 0 & 0 & N_1 & 0 & 0 & N_2 & 0 & 0 & N_3 & 0 & 0 & N_4 \end{bmatrix}. \tag{22}$$

Because the penalty function method is employed to minimize the difference between $\bar{\omega}_z$ and the physical rotation derived from displacement $\bar{\mathbf{u}}$, the physical rotation can be approximately replaced by $\bar{\omega}_z$ for the finite element implementation. Therefore, the test function for symmetric curvature can be expressed as:

$$\bar{\boldsymbol{\chi}} = \begin{Bmatrix} 2\bar{\chi}_{xz} \\ 2\bar{\chi}_{yz} \end{Bmatrix} = \begin{Bmatrix} \dfrac{\partial \bar{\omega}_z}{\partial x} \\ \dfrac{\partial \bar{\omega}_z}{\partial y} \end{Bmatrix} = \bar{\mathbf{B}}^c \mathbf{q}^e , \tag{23}$$

in which

$$\bar{\mathbf{B}}^c = \left[\bar{\mathbf{B}}_1^c \quad \bar{\mathbf{B}}_2^c \quad \bar{\mathbf{B}}_3^c \quad \bar{\mathbf{B}}_4^c \right], \tag{24}$$

$$\bar{\mathbf{B}}_i^c = \begin{bmatrix} 0 & 0 & N_{i,x} \\ 0 & 0 & N_{i,y} \end{bmatrix}, \quad i = 1 \sim 4 . \tag{25}$$

3.2.2 The element's trial functions

Similar to the original US-Q4θ element [1], the trial function for stress of the proposed new element, as work conjugate of the strain test function, is also formulated based on the Airy stress solutions. Since the detailed discussions can be found in [1], the derivation procedure is only briefly summarized here. First, the stress field $\hat{\boldsymbol{\sigma}}$ in Equation (12) is initially assumed as

$$\hat{\boldsymbol{\sigma}} = \begin{Bmatrix} \hat{\sigma}_x \\ \hat{\sigma}_y \\ \hat{\sigma}_{xy} \end{Bmatrix} = \mathbf{H}^n \boldsymbol{\alpha}^n, \tag{26}$$

in which

$$\mathbf{H}^n = \begin{bmatrix} 0 & 0 & 2 & 0 & 0 & 2x & 6y \\ 2 & 0 & 0 & 6x & 2y & 0 & 0 \\ 0 & -1 & 0 & 0 & -2x & -2y & 0 \end{bmatrix}, \tag{27}$$

$$\boldsymbol{\alpha}^n = \begin{bmatrix} \alpha_1 & \alpha_2 & \alpha_3 & \alpha_4 & \alpha_5 & \alpha_6 & \alpha_7 \end{bmatrix}. \tag{28}$$

Secondly, to determine the relations between the unknown coefficients in Equation (28) and the element nodal DOFs in Equation (13), the following quasi-conforming condition is employed:

$$\iint_\Omega \mathbf{H}^{n\mathrm{T}} \left(\overline{\boldsymbol{\varepsilon}} - \mathbf{D}_n^{-1} \hat{\boldsymbol{\sigma}} \right) t \mathrm{d}\Omega = \mathbf{0}, \tag{29}$$

in which $\overline{\boldsymbol{\varepsilon}}$ and $\mathbf{D}_n$ are defined by Equation (18) and Equation (10), respectively. Then, the stress $\hat{\boldsymbol{\sigma}}$ can be rewritten in terms of $\mathbf{q}^e$:

$$\hat{\boldsymbol{\sigma}} = \hat{\mathbf{S}}^n \mathbf{q}^e, \tag{30}$$

in which

$$\hat{\mathbf{S}}^n = \mathbf{H}^n \mathbf{M}_n^{-1} \mathbf{V}_n, \tag{31}$$

with

$$\mathbf{M}_n = \iint_\Omega \mathbf{H}^{n\mathrm{T}} \mathbf{D}_n^{-1} \mathbf{H}^n t \mathrm{d}\Omega, \tag{32}$$

$$\mathbf{V}_n = \iint_\Omega \mathbf{H}^{n\mathrm{T}} \overline{\mathbf{B}}^n t \mathrm{d}\Omega. \tag{33}$$

The trial function for couple stress of the new element, which is work conjugate of the curvature test function as shown in Equation (12), can be obtained by following a similar procedure. The couple stress field $\hat{\mathbf{m}}$ is initially assumed as the following form:

$$\hat{\mathbf{m}} = \begin{Bmatrix} \hat{m}_{xz} \\ \hat{m}_{yz} \end{Bmatrix} = \mathbf{H}^c \boldsymbol{\alpha}^c, \tag{34}$$

in which

$$\mathbf{H}^c = \begin{bmatrix} 1 & 0 & x & 0 & y & 0 \\ 0 & 1 & 0 & x & 0 & y \end{bmatrix}, \tag{35}$$

$$\boldsymbol{\alpha}^c = \left[\alpha_8 \quad \alpha_9 \quad \alpha_{10} \quad \alpha_{11} \quad \alpha_{12} \quad \alpha_{13}\right]. \tag{36}$$

Then, the quasi-conforming technique [51, 52] is employed once again to determine the relation between the unknown coefficients in Equation (36) and the element nodal DOFs, as follows:

$$\iint_\Omega \mathbf{H}^{c\mathrm{T}}\left(\bar{\boldsymbol{\chi}} - \mathbf{D}_c^{-1}\hat{\mathbf{m}}\right) t\mathrm{d}\Omega = \mathbf{0}. \tag{37}$$

Substituting Equation (23) and Equation (34) into Equation (37) yields:

$$\boldsymbol{\alpha}^c = \mathbf{M}_c^{-1}\mathbf{V}_c\mathbf{q}^e, \tag{38}$$

where

$$\mathbf{M}_c = \iint_\Omega \mathbf{H}^{c\mathrm{T}}\mathbf{D}_c^{-1}\mathbf{H}^c t\mathrm{d}\Omega. \tag{39}$$

$$\mathbf{V}_c = \iint_\Omega \mathbf{H}^{c\mathrm{T}}\bar{\mathbf{B}}^c t\mathrm{d}\Omega. \tag{40}$$

Finally, substitution of Equation (38) back into Equation (34) yields

$$\hat{\mathbf{m}} = \hat{\mathbf{S}}^c\mathbf{q}^e, \tag{41}$$

with

$$\hat{\mathbf{S}}^c = \mathbf{H}^c\mathbf{M}_c^{-1}\mathbf{V}_c. \tag{42}$$

It should be noted that, the stress field $\hat{\boldsymbol{\sigma}}$ defined in Equation (30) and the couple stress field $\hat{\mathbf{m}}$ defined in Equation (41) can satisfy *a prior* the related governing equations, making them a good choice for the stress interpolation.

3.2.3 The penalty function

Since the test function for rotation $\bar{\omega}_z$ is independently interpolated by the element nodal drilling DOFs, as shown in Equation (21), it differs from the physical rotation derived from the displacement $\bar{\mathbf{u}}$. Specifically, Λ in Equation (12) has the following expression:

$$\Lambda = \frac{1}{2}\left(\frac{\partial\bar{v}}{\partial x} - \frac{\partial\bar{u}}{\partial y}\right) - \bar{\omega}_z. \tag{43}$$

By substituting Equation (14) and Equation (21) into Equation (43), we can rewrite it as

$$\Lambda = \bar{\mathbf{N}}^\Lambda\mathbf{q}^e, \tag{44}$$

with

$$\bar{\mathbf{N}}^{\Lambda}=\left[\bar{\mathbf{N}}_1^{\Lambda} \quad \bar{\mathbf{N}}_2^{\Lambda} \quad \bar{\mathbf{N}}_3^{\Lambda} \quad \bar{\mathbf{N}}_4^{\Lambda}\right], \tag{45}$$

$$\bar{\mathbf{N}}_i^{\Lambda}=\frac{1}{2}\left[-N_{i,y} \quad N_{i,x} \quad \frac{1}{2}N_{i,x}\left(x-x_i\right)+\frac{1}{2}N_{i,y}\left(y-y_i\right)-N_i\right], \quad i=1\sim 4 . \tag{46}$$

The penalty function method is used in this work to enforce the constraint $\Lambda=0$. The penalty parameter should be set large enough to enforce the constraint at an acceptable level and in general, the constraint will be satisfied more strictly as the penalty parameter k increases. According to dimensional analysis, the penalty parameter k should be proportional with *G*. Parameter studies have been performed to test the influence of the penalty parameter with respect to mesh size and mesh distortion. The numerical results indicate that the solutions are independent from the penalty parameter when $k/G \geq 10^4$. On the other hand, the penalty parameter should not be overly large because it may make the stiffness matrix ill conditioned. Therefore, it is suggested to keep the ratio k/G less than 10^7.

3.2.4 The element stiffness matrix

By substituting the related equations into the virtual work principle in Equation (12), the element stiffness matrix and the equivalent nodal load vector can be obtained as:

$$\mathbf{K}^e=\iint_{\Omega}\bar{\mathbf{B}}^{n\mathrm{T}}\hat{\mathbf{S}}^n t\mathrm{d}\Omega+\iint_{\Omega}\bar{\mathbf{B}}^{c\mathrm{T}}\hat{\mathbf{S}}^c t\mathrm{d}\Omega+k\iint_{\Omega}\bar{\mathbf{N}}^{\Lambda\mathrm{T}}\bar{\mathbf{N}}^{\Lambda}t\mathrm{d}\Omega , \tag{47}$$

$$\mathbf{P}^e=\iint_{\Omega}\bar{\mathbf{N}}^{\mathrm{T}}\mathbf{f}t\mathrm{d}\Omega+\int_{\Gamma}\bar{\mathbf{N}}^{\mathrm{T}}\mathbf{R}t\mathrm{d}\Gamma+\int_{\Gamma}\bar{\mathbf{N}}^{\omega\mathrm{T}}M_z t\mathrm{d}\Gamma . \tag{48}$$

After solving the element nodal DOFs $\mathbf{q}^e$, the stress and couple stress at an arbitrary point within the element can be calculated using Equation (30) and Equation (41).

Note that, as the independently assumed rotation $\bar{\omega}_z$ and the physical rotation derived from displacements have different orders of interpolation, severe locking behavior may be observed when full-integration scheme is used for the last penalty stiffness in Equation (47). To overcome this problem, the selective reduced integration procedure suggested in [39] is employed here: the last penalty term is calculated by using the one-point Gauss quadrature strategy, whilst other integrations are operated by using the full quadrature scheme.

4. Numerical Validation

In this section, several benchmark problems are solved to examine the performance of the proposed element US-Q4θ-CS for modeling the size effect. The penalty parameter is set as $k/G=10^5$ in all benchmark tests, except where otherwise stated.

4.1. The test for rigid body rotation

Figure 2 shows a square block with an edge length $L=\sqrt{2}$ mm modeled by using four elements. To produce a rigid body rotation, two cases with different boundary conditions are considered. The first one is to make $u_1=v_1=0$ and $\theta_1=0.1$ at the central node 1, and the second is to make $u_1=v_1=0$ at node 1 while $v_2=0.1$mm at node 2. In the context of small deformation problems, the rotational angles should be 0.1 at all nodes in these two cases. The numerical results listed in Table 1 verify that the proposed new element can correctly reproduce the rigid body rotation motions.

4.2. The cantilever thin beam

As shown in Figure 3, the benchmark proposed in [54] is solved, in which the cantilever thin beam is subjected to a tip shear load. The reference flexural rigidity for the modified couple stress theory is given by [54]:

$$D_{\mathrm{CS}}=\frac{1}{bh^3}\left(\frac{EI}{1-\mu^2}+GAl^2\right), \tag{49}$$

where A is the cross-sectional area and I is the area moment of inertia. The flexural rigidity obtained by finite element analysis can be evaluated by

$$D_{\mathrm{FEM}}=\frac{PL^3}{3v_{\max}bh^3}, \tag{50}$$

in which $v_{\max}$ is the maximum vertical tip displacement.

First, the convergence properties of the new element are tested. The beam height h is set as 20μm. Three cases with different material length scale parameters l=17.6μm, 13.2μm and 8.8μm are considered. The computations are repeated by successively refining the basic mesh 1×10 given in Figure 4(a) into 2×20, 4×40 and 8×80. The relative errors of the flexural rigidity are shown in Figure 5, in which the results from another 4-node 12-DOF quadrilateral element proposed by

Garg and Han [39] are also plotted for comparison. It can be observed that Garg and Han's element experiences the locking problem in the coarse mesh 1×10. The main reason for this is the element's displacements are interpolated by the standard isoparametric interpolation. In contrast, the proposed element US-Q4θ-CS converges very rapidly and is free of shear locking.

Secondly, the influence from mesh distortion is checked by using the distorted meshes as illustrated in Figure 4(b) and Figure 4(c). The beam height h is 20μm, the material length scale parameters l is 17.6μm and the distortion parameter Δ is set as 10μm. As shown by the results in Figure 6, the new element can also converge well in distorted meshes.

Moreover, to further assess the new element's robustness to mesh distortion, the coarse trapezoidal mesh 1×10 is tested again, by varying the distortion parameter Δ from -20μm to 20μm. Figure 7 shows the variation of the normalized flexural rigidity with respect to the distortion parameter. It can be seen that the maximum deviation is less than 4%, confirming that the proposed new element has low susceptibility to mesh distortion.

Next, the influence on the flexural rigidity from the structure size is studied by using the refined regular mesh 4×40. Four different values of height h=20μm, 38μm, 75μm and 115μm are examined. As shown in Figure 8 and Table 2, the numerical results are in good agreements with the theoretical reference values, proving that this new element can effectively capture the size effects.

Finally, parametric studies are performed to assess the influence of the penalty parameter on the numerical results with respect to mesh size and mesh distortion. The material and dimension parameters are set as h=20μm and l=17.6μm. The ratio of penalty parameter k to shear modulus G is varied from 10 to 10^7. Table 3 lists the results obtained by using regular meshes with different mesh sizes, while Table 4 summarizes the results obtained by using the three distorted meshes 1×10 shown in Figure 4. It can be concluded that the solutions are independent from the penalty parameter when the ratio $k/G \geq 10^4$.

4.3. The simple shear problem

As shown in Figure 9, a slender rectangular panel is clamped from the bottom. On the top surface, the y- direction displacement and rotation are restrained while the x- direction displacement is constrained to the prescribed constant value U=1μm. The analytical solution for the modified

couple stress theory has been obtained Park and Gao [55]:

$$u(y) = C_1 + C_2 y + C_3 e^{\frac{2}{l}y} + C_4 e^{-\frac{2}{l}y}, \tag{51}$$

$$v = 0, \tag{52}$$

in which

$$\begin{cases} C_1 = \dfrac{\alpha}{2}\left(e^{-\frac{2}{l}h} + e^{\frac{2}{l}h} - 2 \right), & C_3 = \dfrac{\alpha}{2}\left(1 - e^{-\frac{2}{l}h} \right) \\ C_2 = \dfrac{\alpha}{l}\left(e^{-\frac{2}{l}h} - e^{\frac{2}{l}h} \right), & C_4 = \dfrac{\alpha}{2}\left(1 - e^{\frac{2}{l}h} \right) \end{cases}, \tag{53}$$

$$\alpha = \frac{U}{\left[-2 + \left(1 + \dfrac{h}{l} \right) e^{-\frac{2}{l}h} + \left(1 - \dfrac{h}{l} \right) e^{\frac{2}{l}h} \right]}. \tag{54}$$

and l is the material length scale parameter. Accordingly, the analytical shear strain can be expressed as follows

$$\gamma_{xy} = C_2 + \frac{2}{l} C_3 e^{\frac{2}{l}y} - \frac{2}{l} C_4 e^{-\frac{2}{l}y}. \tag{55}$$

This rectangle is meshed into 10×100 elements and three different material length scale parameters, i.e., l=176μm, 17.6μm and 8.8μm, are considered. Figures 10 and 11 present respectively the displacement u and the shear strain γ_{xy} along the y- axis. The numerical results agree well with the reference solutions, confirming once again that the proposed new element can correctly capture the size effects.

4.4. The square plate with a hole

In this example, a large square plate containing a circular hole is loaded by uniform uniaxial tension, as shown in Figure 12. Owing to symmetry, only a quarter of the structure is modeled and the corresponding symmetric boundary conditions are applied. Figure 13 shows the meshes employed for FE analysis.

Figure 14 shows the stress concentration factors for different ratios of the material length scale parameter to the hole radius. It is observed that the stress concentration factor decreases with as the length scale parameter decreases. Moreover, the stress σ_x and the couple stress m_x in the vicinity of the hole are obtained by using 512 elements, as shown in Figure 15 and Figure 16. It can be observed that as the material length scale parameter increases, the couple stress concentration

becomes more pronounced whist the stress concentration phenomenon is relieved.

4.5. The bracket

The bracket model proposed in [54] is modified in this study to assess the performance of the new element for practical FE analysis. As shown in Figure 17, the bracket is fixed at its left hole while the right hole is constrained with a vertical displacement U. To study the size effect, two cases with different material length scale parameters l=176μm and 17.6μm are considered. The shear stress σ_{xy} and the couple stress m_x calculated using 1822 elements are plotted in Figures 18 and 19, respectively. It can be observed that, as the material length scale parameter increases, the shear stress reduces in magnitude while the couple stress increases, implying that the couple stress plays an increasingly significant role in energetics.

5. Conclusions

In this paper, an unsymmetric 4-node 12-DOF quadrilateral membrane element is proposed for the modified couple stress theory. The new element is directly developed from the high-performance element model US-Q4θ with drilling DOFs [1]. Specifically, the nodal drilling DOFs in the original US-Q4θ element formulations are constrained by the penalty function method to approximate the physical rotation. Therefore, the test function for the symmetric curvature can be simply derived from these nodal drilling DOFs. Meanwhile, the trial function for the couple stress, which conjugates with the curvature test function, is formulated following the analytical trial function method. To overcome the locking problem, the penalty stiffness term is evaluated by using the one-point Gauss integration strategy. The proposed new element, named as US-Q4θ-CS, has the following characteristics:

(i) This element is developed within the framework of the unsymmetric finite element method. The construction procedure is straightforward and the resulting element formulation is concise. Numerical benchmarks verify that this element can effectively simulate the size-dependent responses with good robustness to mesh distortions.

(ii) According to dimensional analysis, the penalty parameter k should be proportional with G. Parametric studies have been performed to test the influence of the penalty parameter with respect to mesh size and mesh distortion. The numerical results indicate that the solutions are

independent from the penalty parameter when $k/G \geq 10^4$ for all cases tested in this work. Thus, this value can be regarded as an approximate lower limit for the penalty parameter. Moreover, the penalty parameter should not be too large because it may make the stiffness matrix ill conditioned. It is suggested that the value of k/G is set as less than 10^7.

(iii) Different from Garg and Han's 4-node 12-DOF element [39] in which the rotation DOFs are used only to approximate the physical rotation, the proposed new element employs the nodal rotation DOFs not only to determine the test function for physical rotation but also to enhance the test function for displacement. Besides, the new element's trial functions for stress and couple stress are designed using the analytical functions which can *a prior* satisfy the equilibrium equations. Numerical results show that the proposed new element has much better performance than Garg's model, and is free of shear locking in beam bending problems.

(iv) Compared with those elements [31-36] that employ both displacements and displacement derivatives as nodal DOFs, the proposed new element has only three conventional DOFs per node. Thus, it is computationally cheaper at the element level and can be readily incorporated into the standard finite element program for practical applications. For instance, this element can be easily implemented in the commonly used commercial software Abaqus [56] through the user-defined element (UEL) subroutine.

(v) This new unsymmetric element is directly developed from the virtual work principle. It can be further extended to nonlinear analysis by using the incremental form and adopting an appropriate algorithm for updating the stress trial functions [46]. The related topic will be discussed in our future papers.

Acknowledgements

The authors would like to thank for the financial supports from the National Natural Science Foundation of China (Grant numbers 11702133, 11872229) and the Natural Science Foundation of Jiangsu Province (Grant number BK20170772).

References

[1] Shang Y, Ouyang W. 4-node unsymmetric quadrilateral membrane element with drilling DOFs

insensitive to severe mesh-distortion. International Journal for Numerical Methods in Engineering 2018; 113(10): 1589-1606

[2] Fleck NA, Muller GM, Ashby MF, Hutchinson JW. Strain gradient plasticity: Theory and experiment. Acta Metallurgica et Materialia 1994; 42(2): 475-487.

[3] Lam DCC, Yang F, Chong ACM, et al. Experiments and theory in strain gradient elasticity. Journal of the Mechanics and Physics of Solids 2003; 51(8): 1477-1508.

[4] Nix WD, Gao H. Indentation size effects in crystalline materials: A law for strain gradient plasticity. Journal of the Mechanics and Physics of Solids 1998; 46(3): 411-425.

[5] Stelmashenko NA, Walls MG, Brown LM, Milman YV. Microindentations on W and Mo oriented single crystals: An STM study. Acta Metallurgica et Materialia 1993; 41(10): 2855-2865.

[6] Stölken JS, Evans AG. A microbend test method for measuring the plasticity length scale. Acta Materialia 1998; 46(14): 5109-5115.

[7] Han CS. Influence of the molecular structure on indentation size effect in polymers. Materials Science and Engineering A 2010; 527(3): 619-624.

[8] Han CS, Svetoslav N. Indentation size effects in polymers and related rotation gradients. Journal of Materials Research 2007; 22(6): 1662-1672.

[9] Cosserat E. Theorie des Corps deformables. Herman Et Fils Paris 1909.

[10] Mindlin RD. Micro-structure in linear elasticity. Archive for Rational Mechanics and Analysis 1964; 16(1): 51-78.

[11] Mindlin RD, Eshel NN. On first strain-gradient theories in linear elasticity. International Journal of Solids and Structures 1968; 4(1): 109-124.

[12] Fleck NA, Hutchinson JW. Strain gradient plasticity. Advances in Applied Mechanics 1997; 33: 295-361.

[13] Aifantis EC. On the microstructural origin of certain inelastic models. Journal of Engineering Materials and Technology 1984; 106(4): 326-330.

[14] Koiter WT. Couple-stress in the theory of elasticity. Procknedakadwet 1964; 67: 17-44.

[15] Mindlin RD, Tiersten HF. Effects of couple-stresses in linear elasticity. Archive for Rational Mechanics and Analysis 1962; 11(1): 415-448.

[16] Toupin RA. Elastic materials with couple-stresses. Archive for Rational Mechanics and Analysis 1962; 11(1): 385-414.

[17] Hadjesfandiari AR, Dargush GF. Couple stress theory for solids. International Journal of Solids and Structures 2011; 48(18): 2496-2510.

[18] Aifantis EC. On the role of gradients in the localization of deformation and fracture. International Journal of Engineering Science 1992; 30(10): 1279-1299.

[19] Altan BS, Aifantis EC. On some aspects in the special theory of gradient elasticity. Journal of the Mechanical Behavior of Materials 1997; 8(3): 231-282.

[20] Fleck NA, Hutchinson JW. A phenomenological theory for strain gradient effects in plasticity. Journal of the Mechanics and Physics of Solids 2001; 41(12): 1825-1857.

[21] Yang F, Chong ACM, Lam DCC, Tong P. Couple stress based strain gradient theory for elasticity. International Journal of Solids and Structures 2002; 39(10): 2731-2743.

[22] Vu-Quoc L, Tan X. Efficient Hybrid-EAS solid element for accurate stress prediction in thick laminated beams, plates, and shells. Computer Methods in Applied Mechanics and Engineering 2013; 253: 337-355.

[23] Shu JY, King WE, Fleck NA. Finite elements for materials with strain gradient effects. International Journal for Numerical M ethods in Engineering 2015; 44(3): 373-391.

[24] Deng G, Dargush GF. Mixed Lagrangian formulation for size-dependent couple stress elastodynamic and natural frequency analyses. International Journal for Numerical Methods in Engineering 2017; 109(6): 809-836.

[25] Chen J, Li CJ. A quadrilateral spline element for couple stress/strain gradient elasticity. Computers & Structures 2014; 138: 133-141.

[26] Zhang B, He YM, Liu DB, et al. A non-classical Mindlin plate finite element based on a modified couple stress theory. European Journal of Mechanics A/Solids 2013; 42: 63-80.

[27] Ma H, Gao XL, Reddy J. A non-classical Mindlin plate model based on a modified couple stress theory. Acta Mechanica 2011; 220(1-4): 217-235.

[28] Zervos A, Papanicolopulos SA, Vardoulakis I. Two finite-element discretizations for gradient elasticity. Journal of Engineering Mechanics 2009; 135(3): 203-213.

[29] Papanicolopulos SA, Zervos A, Vardoulakis I. A three dimensional C^1 finite element for gradient elasticity. International Journal for Numerical Methods in Engineering 2010; 77(10): 1396-1415.

[30] Kwon YR, Lee BC. A mixed element based on Lagrange multiplier method for modified couple stress theory. Computational Mechanics 2017; 59(1): 117-128.

[31] Ma X, Chen W. Refined 18-DOF triangular hybrid stress element for couple stress theory. Finite Elements in Analysis and Design 2013; 75: 8-18.

[32] Ma X, Chen W. 24-DOF quadrilateral hybrid stress element for couple stress theory. Computational Mechanics 2014; 53(1): 159-172.

[33] Zhao J, Chen W, Ji B. A weak continuity condition of FEM for axisymmetric couple stress theory and an 18-DOF triangular axisymmetric element. Finite Elements in Analysis and Design 2010; 46(8): 632-644.

[34] Zhao J, Chen WJ, Lo SH. A refined nonconforming quadrilateral element for couple stress/strain gradient elasticity. International Journal for Numerical Methods in Engineering 2011; 85(3): 269-288.

[35] Wang CS, Zhang XK, Hu P. A 4-node quasi-conforming quadrilateral element for couple stress theory immune to distorted mesh. Computers & Structures 2016; 175: 52-64.

[36] Wang CS, Zhang XK, Hu P. Assumed stress quasi-conforming triangular element for couple stress theory. Acta Mechanica Solida Sinica 2017; 30(4): 335-344.

[37] Xia ZC, Hutchinson JW. Crack tip fields in strain gradient plasticity. Journal of the Mechanics and Physics of Solids 1996; 44(10): 1621-1648.

[38] Shu J, Fleck N. The prediction of a size effect in microindentation. International Journal of Solids and

Structures 1998; 35(13): 1363-1383.

[39] Garg N, Han CS. A penalty finite element approach for couple stress elasticity. Computational Mechanics 2013; 52(3): 709-720.

[40] Chakravarty S, Hadjesfandiari AR, Dargush GF. A penalty-based finite element framework for couple stress elasticity. Finite Elements in Analysis and Design 2017; 130: 65-79.

[41] Darrall BT, Dargush GF, Hadjesfandiari AR. Finite element Lagrange multiplier formulation for size-dependent skew-symmetric couple-stress planar elasticity. Acta Mechanica 2014; 225(1): 195-212.

[42] Rajendran S, Liew K. A novel unsymmetric 8-node plane element immune to mesh distortion under a quadratic displacement field. International Journal for Numerical Methods in Engineering 2003; 58(11): 1713-1748.

[43] Ooi ET, Rajendran S, Yeo JH. Extension of unsymmetric finite elements US-QUAD8 and US-HEXA20 for geometric nonlinear analyses. Engineering Computations 2007; 24(4): 407-431.

[44] Cowan T, Coombs WM. Rotationally invariant distortion resistant finite-elements. Computer Methods in Applied Mechanics and Engineering 2014; 275: 189-203.

[45] Huang JB, Cen S, Li Z, Li CF. An unsymmetric 8-node hexahedral solid-shell element with high distortion tolerance: Linear formulations. International Journal for Numerical Methods in Engineering 2018; DOI:10.1002/nme.5945.

[46] Li Z, Cen S, Wu CJ, et al. High-performance geometric nonlinear analysis with the unsymmetric 4-node, 8-DOF plane element US-ATFQ4. International Journal for Numerical Methods in Engineering 2018; 114(9): 931-954.

[47] Zhou PL, Cen S, Huang JB, et al. An unsymmetric 8-node hexahedral element with high distortion tolerance. International Journal for Numerical Methods in Engineering 2017; 109(8): 1130-1158.

[48] Cen S, Zhou PL, Li CF, Wu CJ. An unsymmetric 4-node, 8-DOF plane membrane element perfectly breaking through MacNeal's theorem. International Journal for Numerical Methods in Engineering 2015; 103(7): 469-500.

[49] Xie Q, Sze KY, Zhou YX. Modified and Trefftz unsymmetric finite element models. International Journal of Mechanics and Materials in Design 2016; 12(1): 53-70.

[50] Fu XR, Cen S, Li C, Chen XM. Analytical trial function method for development of new 8-node plane element based on the variational principle containing Airy stress function. Engineering Computations 2010; 27(4): 442-463.

[51] Tang LM, Chen WJ, Liu YX. Quasi-conforming elements for finite element analysis. Journal of Dalian University of Technology 1980; 19(2): 17-35. (in Chinese)

[52] Chen WJ, Liu YX, Tang LM. The formulation of quasi-conforming elements. Journal of Dalian University of Technology 1980; 19(2): 37-49. (in Chinese)

[53] Hadjesfandiari AR, Dargush GF. Couple stress theory for solids. International Journal of Solids and Structures 2011; 48(18): 2496-2510.

[54] Choi JH, Lee BC. A three-node C^0 triangular element for the modified couple stress theory based on the smoothed finite element method. International Journal for Numerical Methods in Engineering 2018;

114(12): 1245-1261.

[55] Park SK, Gao XL. Variational formulation of a modified couple stress theory and its application to a simple shear problem. Zeitschrift Für Angewandte Mathematik Und Physik 2008; 59(5): 904-917.

[56] Abaqus 6.9. HTML Documentation, Dassault Systèmes Simulia Corp, Providence, RI, USA, 2009.

Table 1. Rotation results of the test for rigid body rotation

	Node	1	2	3	4	5
θ	Case A	0.1	0.1	0.1	0.1	0.1
	Case B	0.1	0.1	0.1	0.1	0.1

Table 2. The relative errors of flexural rigidity using the regular mesh 4×40

	h=20μm	h=38μm	h=75μm	h=115μm
l=17.6μm	0.127%	0.686%	1.065%	1.154%
l=13.2μm	0.386%	0.881%	1.132%	1.175%
l= 8.8μm	0.725%	1.064%	1.173%	1.186%

Table 3. The normalized flexural rigidity with different penalty parameters and different mesh sizes of the regular mesh (h=20μm and l=17.6μm)

k/G	10	10^2	10^3	10^4	10^5	10^6	10^7
1×10	1.00627	1.00673	1.00678	1.00678	1.00678	1.00678	1.00678
2×20	1.00240	1.00278	1.00282	1.00283	1.00283	1.00283	1.00283
4×40	0.99974	1.00090	1.00122	1.00127	1.00127	1.00127	1.00127
8×80	0.99863	0.99989	1.00016	1.00019	1.00019	1.00019	1.00019

Table 4. The normalized flexural rigidity with different penalty parameters and different basic meshes 1×10 (h=20μm and l=17.6μm)

k/G	10	10^2	10^3	10^4	10^5	10^6	10^7
Mesh (a)	1.00627	1.00673	1.00678	1.00678	1.00678	1.00678	1.00678
Mesh (b)	1.02515	1.02562	1.02567	1.02568	1.02568	1.02568	1.02568
Mesh (c)	1.01206	1.01251	1.01256	1.01256	1.01256	1.01256	1.01256

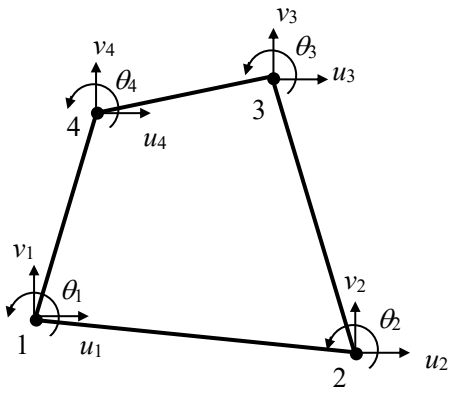

Figure 1. Unsymmetric 4-node 12-DOF quadrilateral membrane element

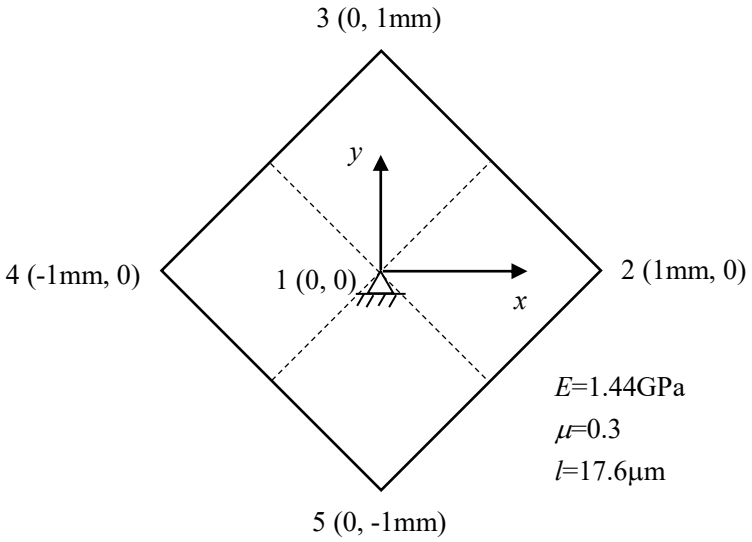

Figure 2. The test for rigid body rotation

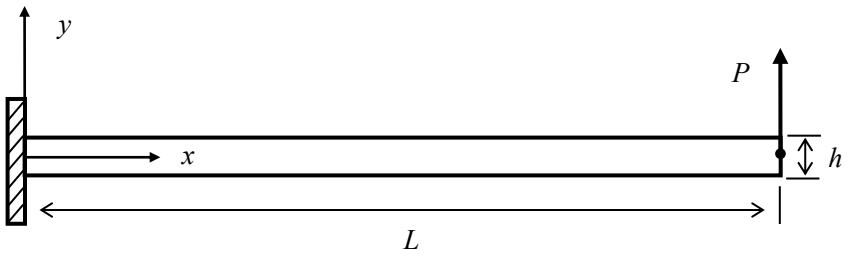

E=1.44GPa, μ=0.38, L=20h, width b=2h, P=100μN

Figure 3. The micro cantilever thin beam

(a) Regular mesh

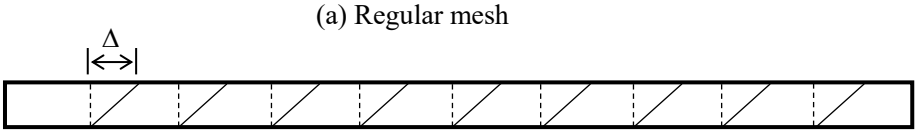

(b) Parallelogram mesh

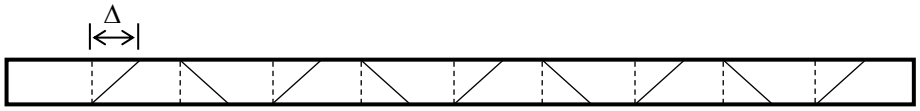

(c) Trapezoidal mesh

Figure 4. Three typical basic meshes 1×10 for the micro cantilever thin beam

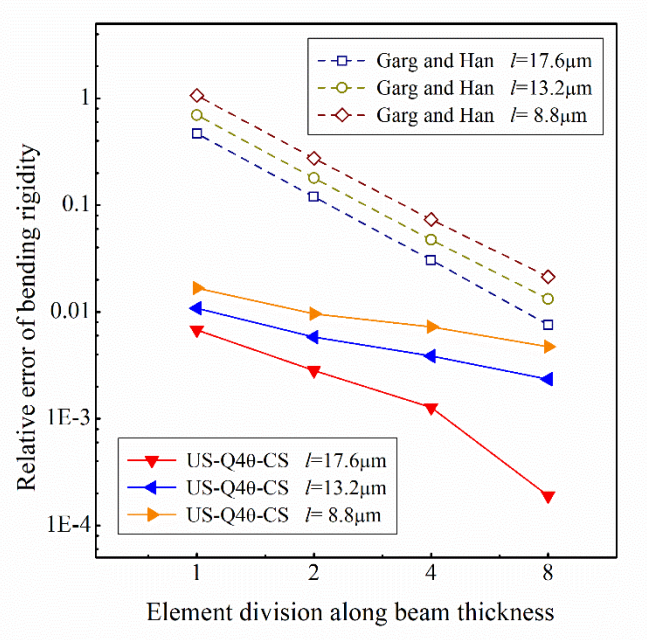

Figure 5. The relative errors of flexural rigidity using the regular mesh shown in Figure 4(a) with h=20μm

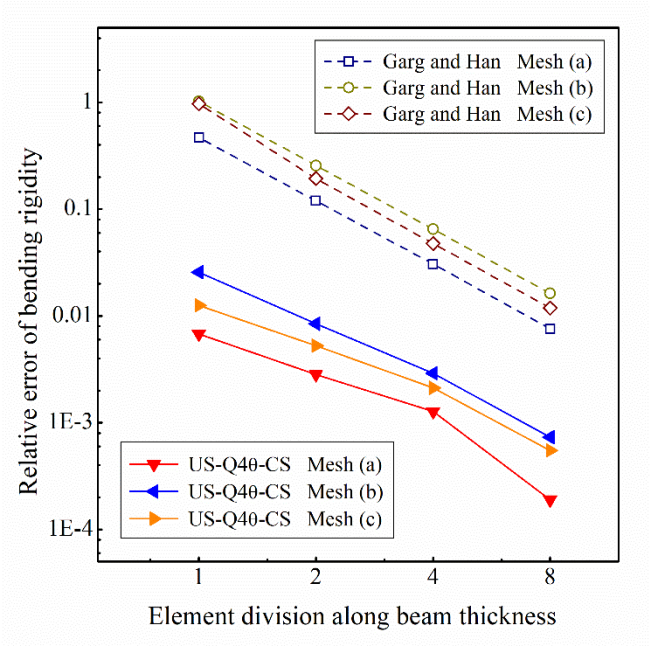

Figure 6. The relative errors of flexural rigidity using different distorted meshes (h=20μm, l=17.6μm and Δ=10μm)

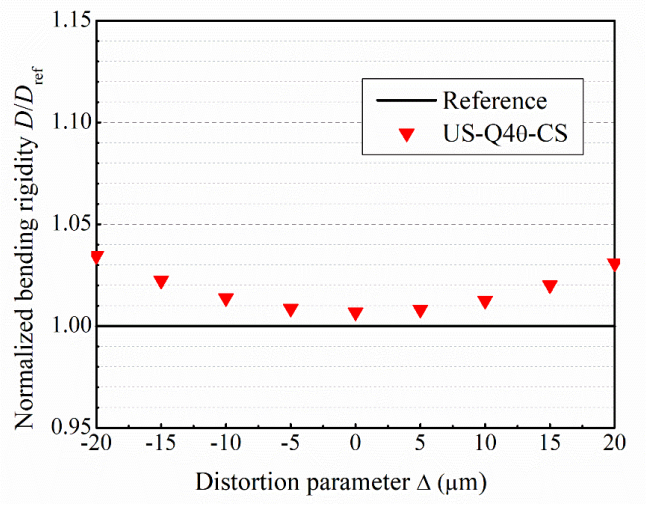

Figure 7. The normalized flexural rigidity versus the distortion parameter using the trapezoidal mesh 1×10 with h=20μm and l=17.6μm

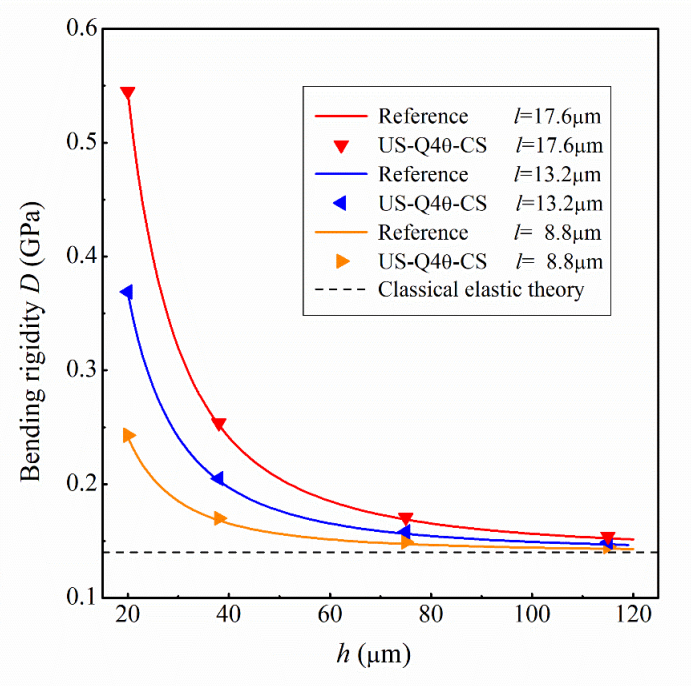

Figure 8. The flexural rigidity versus the beam thickness using the regular mesh 4×40

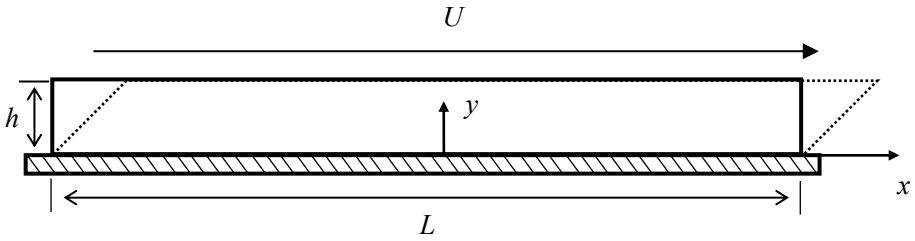

E=1.44GPa, μ=0.38, h=100μm, L=10h, width b=10h, U=1μm

Figure 9. The simple shear problem

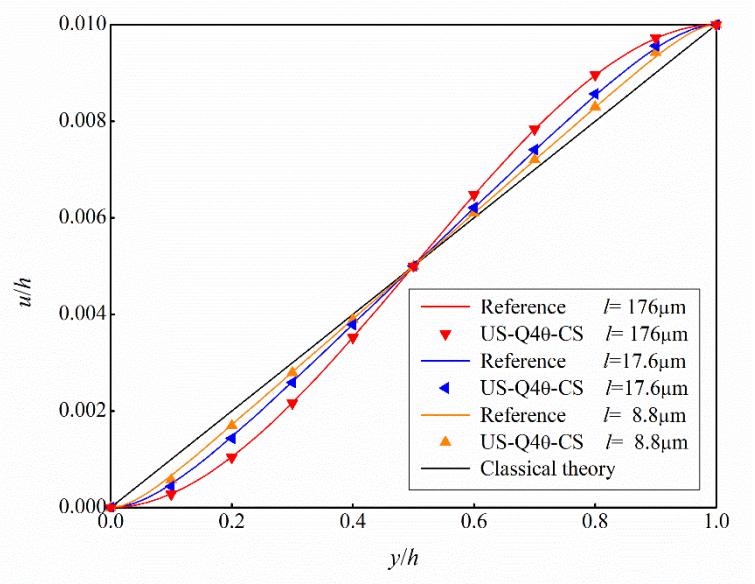

Figure 10. Distribution of displacement u along x=0 of the simple shear problem using the mesh 10×100

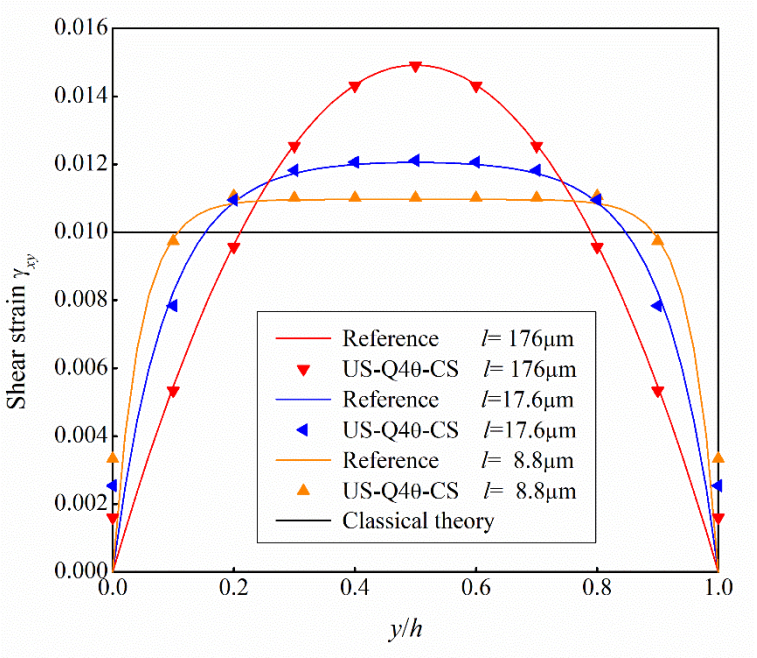

Figure 11. Distribution of shear strain γ_{xy} along x=0 of the simple shear problem using the mesh 10×100

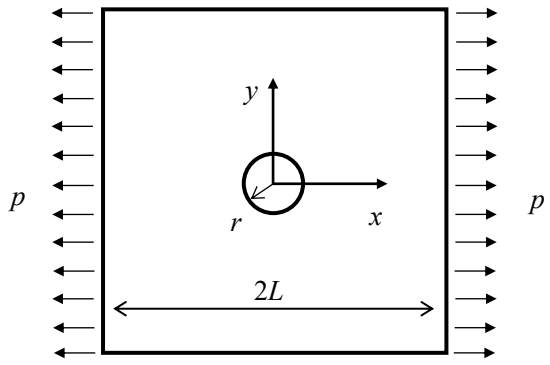

E=1.44GPa, μ=0.3, r=0.1mm, L=3.6mm, width b=10r

Figure 12. Square plate with a hole under uniform tension

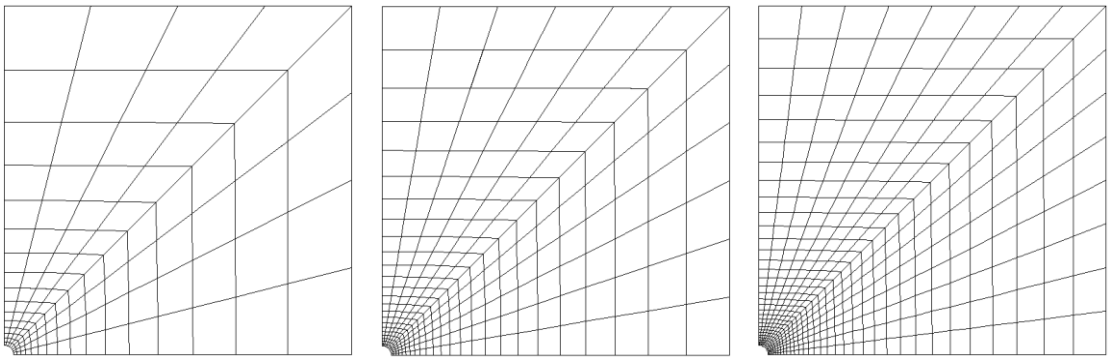

(a) 128 elements (b) 288 elements (c) 512 elements

Figure 13. Meshes used for the square plate with a hole

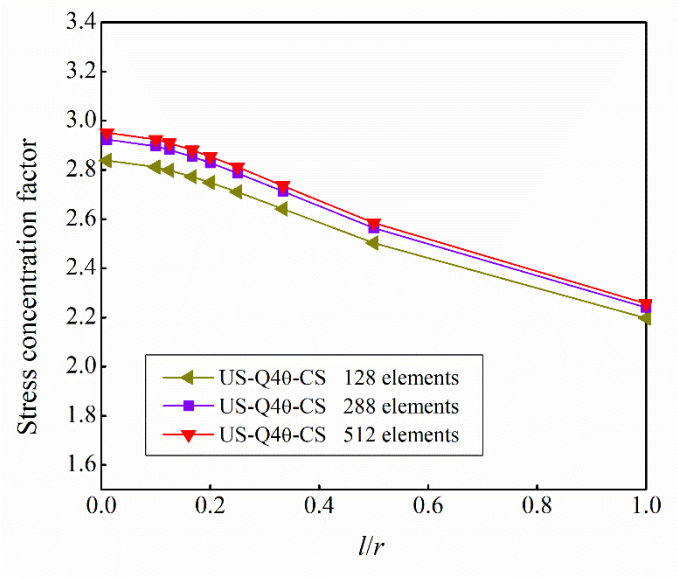

Figure 14. The stress concentration factor versus *l*/*r* obtained by using different meshes

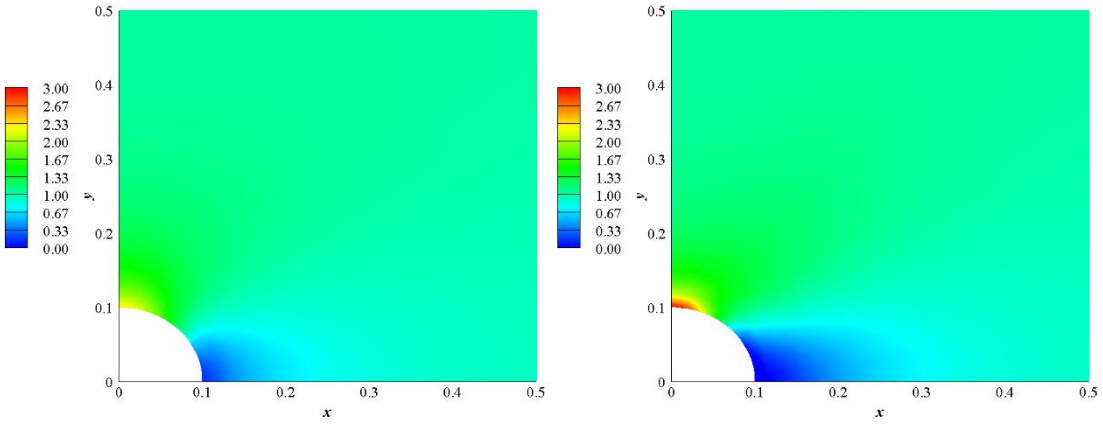

(a) l/r=1 (b) l/r=0.01

Figure 15. The stress σ_x near the hole, obtained by using 512 elements

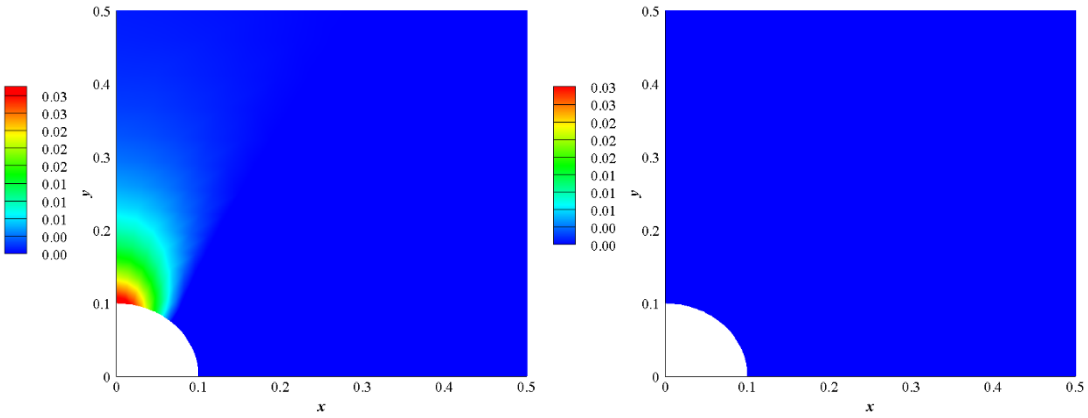

(a) l/r=1 (b) l/r=0.01

Figure 16. The couple stress m_x near the hole, obtained by using 512 elements

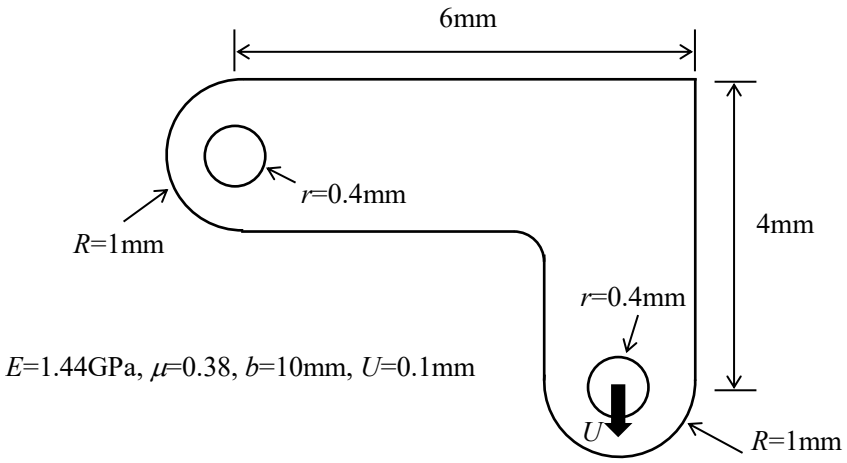

Figure 17. The geometry of the bracket

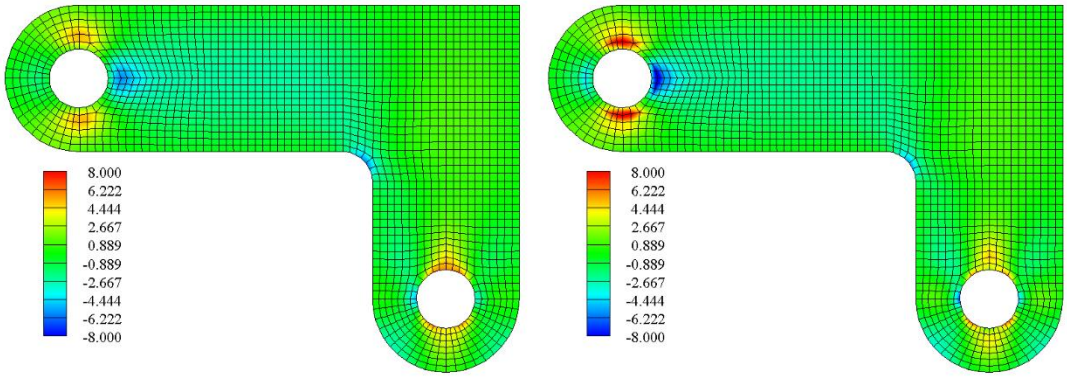

(a) l=176μm (b) l=17.6μm

Figure 18. The shear stress σ_{xy} of the bracket

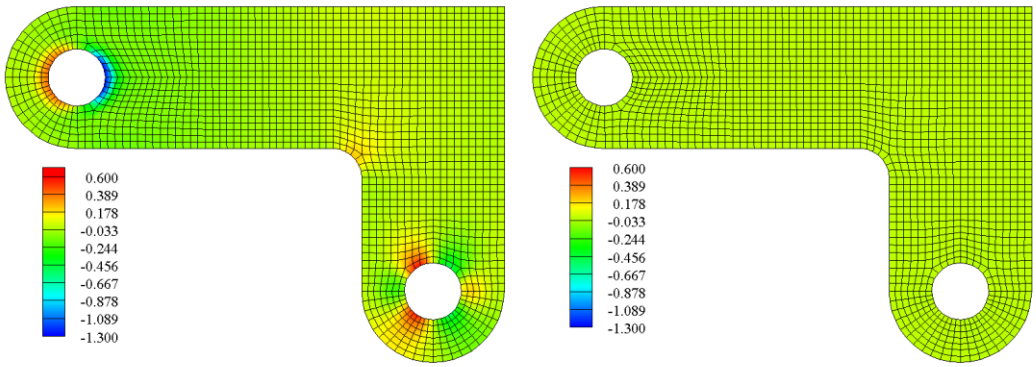

(a) l=176μm (b) l=17.6μm

Figure 19. The couple stress m_x of the bracket